DAMAGE CHARACTERIZATION OF COMPOSITE PLATES UNDER LOW VELOCITY IMPACT USING ULTRASONIC GUIDED WAVES

A. De Luca[a], F. Caputo[a], Z Sharif Khodaei[b], M H Aliabadi[b],

a) Department of Industrial and Information Engineering, University of Campania L. Vanvitelli, Via Roma 29, 81031 Aversa, Italy.

b) Department of Aeronautics, Imperial College London, South Kensington Campus, Exhibition Road, SW7 2AZ, London, UK

corresponding author: francesco.caputo@unicampania.it

Keywords: A. Laminates; B. Impact behaviour; C. Finite element analysis (FEA); D. Non-destructive testing; Lamb waves

ABSTRACT

In this work, two numerical procedures based on Finite Elements Method (FEM) have been developed in order to simulate the Lamb wave propagation in Low Velocity Impact (LVI) damaged CFRP (Carbon Fibre Reinforced Polymer) laminate. The former (softening representation), usually adopted in literature, consists of modelling LVI damages by lowering the elastic material properties which allowed investigating the Lamb wave propagation at different stages of LVI damages evolution. The latter, proposed in this paper, conversely to the first one and the most of techniques presented in literature, consists of simulating Lamb wave propagation in a plate characterized by an initial stress-strain state and the related failures carried out by a previous impact simulation involving the same model. Such technique allows a better damage modelling and, consequently, overcoming the damage modelling approximations introduced by the former strategy; the lowering of the elastic material properties leads to a bad damage modelling which does not allow reproducing accurately what happens in the reality. Such procedure allowed investigating the Lamb wave propagation at different impact energy levels.

The interaction between Lamb waves and damages has been investigated under three central frequencies of the actuation signal: 150 kHz, 200 kHz and 250 kHz which resulted in interesting observations to minimize the effect of the first lamina's fibres orientation on the wave propagation velocity. It is well known that different wave propagation velocities along fibres and matrix lead to different RMSD (Root Mean Square Deviation) damage index values, even if the sensors are mounted at the same distance from the damage location, resulting in wrong or less accurate information about the identification of both damage size and location during the post-processing phase. Moreover, the relationships between the RMSD damage index values, recorded at different instants of time of the impact history, and the impactor phases has been achieved. Finally a comparison between the results achieved by the two investigated strategies has been carried out and presented here.

1 Introduction

Experience with structural failures led to several changes in aircraft design practice, especially for conventional materials, such as steel, aluminium alloys and so on. The improvement of the design practice has allowed the modern structures better tolerating the presence of cracks and, in general, damages under the in-service loading conditions. Thanks to the predictive models, assessed and validated by experimental evidence, designers' forecast capability has been improved significantly. Thus, especially in the aerospace field, nowadays, the damage tolerance philosophy is the heart of the current design practice. Conversely to the conventional materials, composite ones, which have found increasing industrial applications in the last decades, especially in the aerospace and transport fields [1], cannot count on established predictive models in support to the damage tolerance approach. This results in the oversizing of the structures which must be enabled to tolerate damages as well as conventional materials.

Concerning composite materials, in particular Carbon Fibre Reinforced Polymers (CFRP) materials, several types of undetectable manufacturing defects and accidental damages could affect the residual strength of the structures [2-6]. Among the several accidental damages, Low Velocity

Impact (LVI) [7-9] ones play a critical role during the current design practice. Following a LVI, such as tool drop or runway debris, the structure may return to its original shape without showing any detectable damages, whilst it has suffered internal massive damages [9] resulting in Barely Visible Impact Damage (BVID) [2, 9]. To fulfil the damage tolerance design targets, several safety factors are applied during the design practice as a function of the damage size (Figure 1). For civil aviation, according to the FAR25/CS25, the AMC 25.571-2.1.2 [10] allows the residual strength of a component in presence of readily-detectable damages to be at load levels lower than the limit load (LL), specified in CS 25.571 (b) [10], and named 85% LL criteria [11]. For immediately detectable damages, where it is assumed that the crew will be aware of the damage and attempt to land as soon as possible after the event, lower residual strength loads criteria can be used (AMC 25.571-2.7.2 [10 named 70% LL criteria) [11].

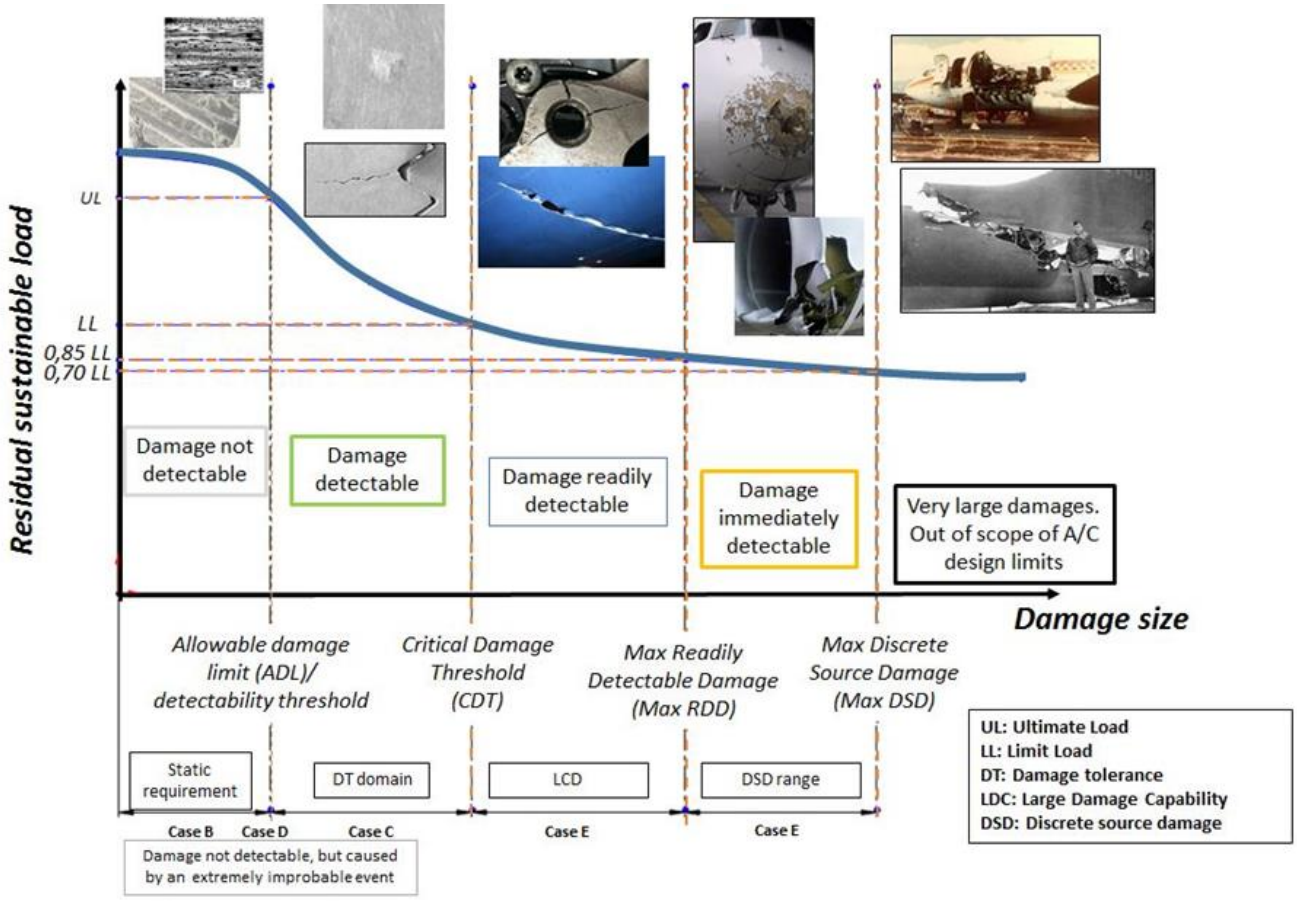

Figure 1. Residual sustainable load vs. damage size.

According to Figure 1, it can be noticed that BVIDs, contained in damage detectable domain, can be tolerated inside the structure as long as its residual strength does not decrease below the limit load. It means that, in order to tolerate damages with a lower detectability level, higher safety factors must be applied. So, nowadays, the interest of the research community is to lower the safety factors related to BVID, by being able to detect them during the in-service life. The main adopted research strategy consists of the development and application of Structural Health Monitoring (SHM) systems for damage detection purpose. The continuous assessment of structural health by means of non-destructive testing (NDT) methods is an important task for the improvement of the damage tolerance philosophy [12]. Among the several techniques, the SHM system based on the propagation of ultrasonic guided wave (Lamb waves), activated by piezoelectric sensors is increasingly being used, due to its durability, light weight and low power consumption. This paper focuses on the LVI damages detection capability of the Lamb wave SHM system in thin CFRP plates.

Such technique is based on the propagation of the guided waves, which are excited by one or more actuators. Once the waves are excited, they propagate through the plate and will be recorded by the sensors attached to the component. The propagation properties of the guided waves depend on the properties of the media they travel through. Therefore, once they interact with a damaged area, the wave reflects and refracts. The interaction of the propagated waves with the damage zone, not only depends on the properties of the damage zone, such as type and size of the damage, but also on the parameters of the excited wave, such as wave mode, shape and central frequency.

Moreover, whilst their propagation in homogenous and isotropic material is well established [12, 13], further investigations are mandatory on non-isotropic materials, especially on dispersion, slowness and attenuation phenomena. In fact, in order to use Lamb waves for diagnostic purpose, they should be characterized by non-dispersion, low attenuation, high sensitivity to damage, easy excitability and good detectability. Also the choice of the right wave modes is important for damage detection purposes.

For such reason, experimental studies on this topic are not sufficient due to the high cost and time consumption of tests and the achievement of a prediction model to investigate on the right parameters which will drive the ultrasonic guided waves in real applications is still an ambitious task for the research community. As matter of the fact, several research activities and several investigation approaches can be found in literature. Such approach can be divided into analytical/semi-analytical, numerical, and experimental works. Numerical method, based on the Finite Element (FE) theory, is widely used in the literature because it allows the prediction of all propagation phenomena and the development of efficient damage detection algorithms. In more detail, both two-dimensional (2D) and three-dimensional (3D) approaches can be adopted. For example, Yelve et al. [14] used 2D FE simulation on Lamb waves based on nonlinear method to detect the delamination in a composite laminate. Mustapha et al. [15] modelled a sandwich structure with 2D composite shell elements to investigate the guided waves propagating behaviour. Hennings et al. [16] also focused on two-dimensional approach for Lamb wave simulation. In their work, the authors showed that thin walled fibres reinforced plastic materials with arbitrary fibres orientation and lay-up or with woven fabrics can be affected by a phenomenon named ‘‘quasi-continuous mode conversion”. Hence, a stochastic inhomogeneity should be implemented into the material law, to improve the modelling technique.

Attributing to the importance of material performance along the thickness direction, Ng et al. [17] discussed the necessity for applying 3D simulation model to test guided waves in composite laminates. However, other authors, e.g. Sharif-Khodaei et al. [18], showed that for thin walled composite plate shell elements (continuum and conventional) and 3D brick elements produce the same results for the first symmetric (S0) and antisymmetric (A0) modes in all investigated numerical models. The discrepancies, which arise later, are attributed to the shorter wavelength of higher modes (A1, S1,…), requiring a higher number of Nodes per Wavelength (NPW).

Wang et al. [19],presented a nonlinear Lamb-wave-based method for fatigue crack detection in steel plates with and without carbon fibres reinforcement polymer (CFRP) modelling both sensors and plate by means of brick finite elements.

According to the literature, the most efficient method adopted for damage detection purpose, based on the wave propagation system, consists of comparison of the baseline signal achieved for undamaged/un-notched structures with the signal achieved in correspondence of the damaged/notched ones.

In this work, two finite element procedures, based on the aforementioned method, have been developed to simulate the guided wave propagation in LVI damaged CFRP laminates. The former, commonly used in literature, consists of modelling LVI damages, and the damages in general, by lowering the elastic material properties. The application of such technique allowed investigating the Lamb wave propagation at different stages of LVI damages evolution. The latter, developed within such research activity, conversely to the first one and to the most of works presented in literature, simulates Lamb wave propagation in a composite plate characterized by an initial stress-strain state and the related failures carried out by a previous impact simulation. Such procedure allowed investigating the interaction of Lamb wave with damage for different impact energy levels. In particular, while the former technique introduces several approximations (the lowering of the elastic material properties does not allow reproducing accurately a real damage configuration), the application of the developed technique allows overcoming such problems and better modelling the interactions between Lamb waves and LVI damages. Under such strategy, in fact, damages are introduced in the plate according to such established criteria as Hashin ones.

2 Lamb waves overview.

Lamb waves are ultrasonic guided waves that propagate in thin plate or shell structures in correspondence to the external surfaces. Lamb waves can be seen as the superimposition of infinite wave modes, which can be mainly classified in two groups: Symmetric, S_i, and Antisymmetric, A_i, wave modes, where the subscript "*i*" (i = 0, 1, 2, …, n) is the wave order [12]. However, in a

medium covered by a layer of different material, such as a multi-layered composite component, new wave modes, named Shear Horizontal, SH_i, modes, can be generated [12]. According to several works [20-28], each wave mode type can be chose to detect a specific damage type. Actually, the S_0 mode appears to be more used for damage identification, differently from the A_0 one, thanks to the following properties:

- lower attenuation than A_0, since the A_0 mode is characterized by out-of-plane displacement and, then, by a more leak of energy;
- faster propagation velocity; it means that complex boundary condition scattered waves can be avoided;
- lower dispersion in the low frequency range.

However, also A_0 mode shows some advantages:

- short wavelength at given excitation frequency;
- larger signal magnitude;
- easier activation.

As a result, S_0 mode shows higher sensitivity to damage in the thickness and to delamination; whereas A_0 mode exhibits higher sensitivity to surface damage, such as surface cracks and surface crack growth [12]. The subscript "*0*" is related to the first recorded waves package.

In addition, exploration of higher-order wave modes has indicated that higher-order modes such as the S_1 mode can be more suitable for finding tiny structural damage, although it is difficult to activate and interpret higher-order waves mode in practice. Moreover, the SH_0 mode has the same sensitivity level as the S_0 mode.

In order to select a wave mode rather than another, different techniques can be adopted; for example, by mounting two PZT (Piezoelectric) sensors at the top and at the bottom of a plate, in order to share the same planar coordinate systems, it is possible to achieve:

- a dominant S_0 mode, with a weak A_0 mode, if the PZT sensors are excited in-phase;

- A_0 mode for the most of the signal, if the two PZT sensors are excited out-of-phase.

In this paper both S_0 and A_0 modes have been considered for the damage detection.

3 FE Model.

As aforementioned, in this work, two finite elements procedures have been considered to simulate the waves propagation in damaged CFRP laminates. The former consists of modelling of LVI damages by lowering the elastic material properties. Such technique allowed investigating the Lamb wave propagation at different stages of LVI damages evolution. In order to model more accurately the LVI damages, a preliminary LVI simulation has been performed. Once the damages configurations for different instants of time of the impact history have been numerically modelled, the following step consisted of the attempt to reproduce them in several analogous plates, as many as the selected damages configurations/instants of time, just by lowering the elastic material properties, ply by ply, in correspondence to the affected zones.

The latter technique consists of the simulation of Lamb waves onto a plate characterized by an initial stress-strain state and the related failures carried out by a previous impact simulation involving the same model. This technique allowed overcoming, rather than the approximations introduced by the former technique, the difficulties relating to the iterative modelling of the impact damages distribution, giving the possibility to investigate the Lamb wave propagation at different impact energy levels. According to both modelling strategies, all damages configurations have been investigated with three “five-cycle sine-burst” actuation signals with central frequencies of 150 kHz, 200 kHz and 250 kHz, respectively. Since both strategies need a previous LVI simulation, the description of the simulations of the impact phenomena, which are based on the same FE approach, is postponed in the following section. As matter of the fact, in all presented Lamb waves FE simulations, no damping factors have been defined in the material properties of the plate, in order to save computational costs. A consequence may be a slight delay between experimental and numerical signals, which is an acceptable approximation for the main goal of this work [18].

3.1 Impact simulation

The numerical model to simulate LVI has been developed by means of Abaqus® 6.14 code [2, 9]. Reduced integration general-purpose shell elements (S4R, from the Abaqus elements' library; 6 degrees of freedom (dofs) per node) have been used to model the plate (200 mm x 200 mm), which consists of 8 laminae (Figure 2.a). Each finite element is characterized by 24 integration points through the thickness, three for each lamina. Orientation and material properties of the laminae have been associated to these points. The stacking sequence (Figure 2.b) of the laminate is a quasi-isotropic one, $[0/90/45/-45]_s$. Laminae are modelled by referring to the material properties shown in Table I. The plate thickness is 2.496 mm.

Table I. Unidirectional lamina material proprieties.

Longitudinal Young Modulus, E_{11}	103.05 GPa	Critical ERR-MODE II, G_{IIIC}	500 J·m^{-2}
Transverse Young Modulus, $E_{22} = E_{33}$	11.55 GPa	Longitudinal tensile strength X_t	1460.7 MPa
In Plane Shear Modulus, $G_{12} = G_{13}$	6 GPa	Longitudinal compressive strength X_c	876.42 MPa
In Plane Shear Modulus, G_{23}	6 GPa	Transverse tensile strength $Y_t = Z_t$	77.145 MPa
Poisson ratio, $v_{12} = v_{13}$	0.312	Transverse compressive strength $Y_c = Z_c$	241.43 MPa
Poisson ratio, v_{23}	0.49	Shear strength $S_{12} = S_{13}$	90 MPa
Critical ERR-MODE I, G_{IC}	180 J·m^{-2}	Shear strength S_{23}	40 MPa
Critical ERR-MODE II, G_{IIC}	500 J·m^{-2}	Ply thickness	0.312 mm

The average characteristic length of the finite elements of the plate model is 0.5 mm. Then, the plate model counts a total of 160801 nodes and 160000 elements. The impactor, modelled by discrete-rigid-elements (R3D4, from the Abaqus elements' library; 3 dofs per node), consists of a 19 mm diameter hemispherical drop mass. The impactor is characterized by an average mesh size equals to 0.3 mm, (27336 nodes and 27334 elements). The penalty contact formulation has been considered for the contact definition between the impactor and the laminate.

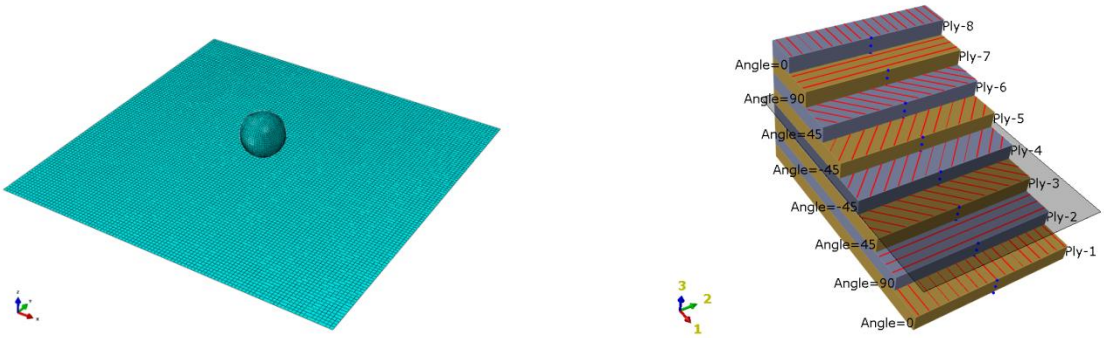

Figure 2. FE model (a) and composite layup (b).

All impact simulations are characterized by a drop mass of 2 kg. Moreover, whilst the impact simulation developed for the first strategy (named in the following “softening representation”) is characterized by an energy level of 25 J, for the second strategy (named in the following “LVI damages representation based on Hashin criteria”), in order to investigate the Lamb wave propagation at different impact energy levels, several impact scenarios have been numerically simulated by changing the initial velocity of the drop mass.

In particular, five different initial velocities of the drop mass have been considered, for different impact energy levels of 5 J, 10 J, 15 J, 20 J and 25 J, respectively. Intra-laminar failures, such as fibre and matrix failures, have been modelled according to Hashin criteria, as shown in [29].

3.2 Wave-damage interaction: softening representation

The first FE modelling strategy aims to understand the propagation mechanisms of Lamb waves during the onset and the evolution of LV impacts. In order to do that, a LVI simulation, with an impact energy level equals to 25 J, has been performed. As described before, after that, the damage configurations at six different impact stages of the impact history have been chosen with the aim to reproduce them in other six separate FE analyses where the Lamb waves will be activated. Damage configurations have been chosen at the time instants 1.5 ms, 1.6 ms, 1.8 ms, 2.0 ms, 2.5 ms and 5.0 ms of the contact force history shown in Figure 3.

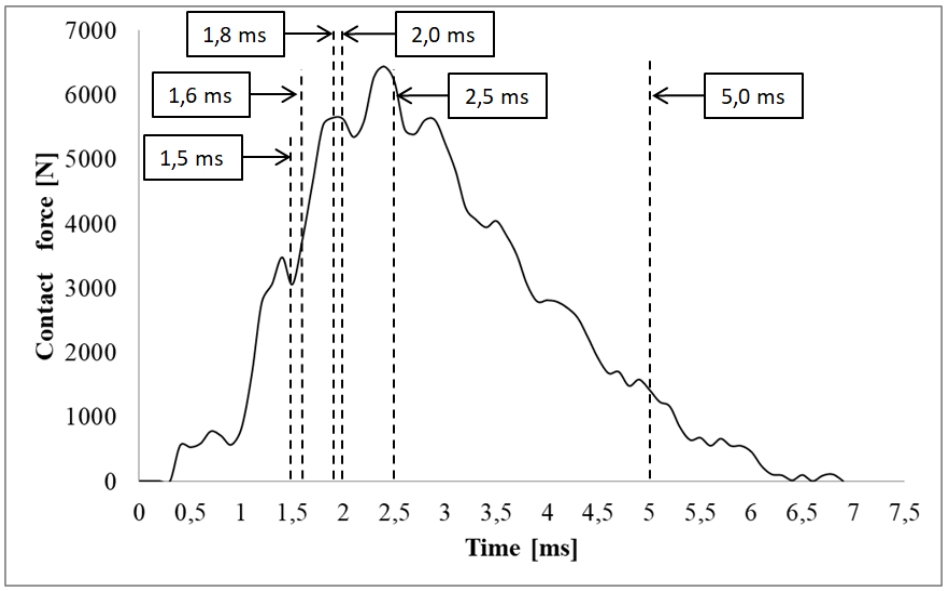

Figure 3. Contact force vs. time.

Damage configurations at the aforementioned time instants have been shown in Tables II and III, by classifying them in matrix and fibre failures, respectively. The tables show the fibres and matrix failures affecting the 8 laminae, respectively. Such damages have been modelled during the impact simulation according to Hashin criteria [29], which allow modelling matrix and fibres failures under tensile and compressive loading conditions, separately [29]. In more detail, the contours plot shown in Tables II and III have been achieved by plotting the finite elements characterized by a level of

damage greater or equal to 80% (the damage level ranges between 0%, for the undamaged configuration, and 100%, for the fully damaged configuration). Hence, according to Tables II and III, the damage level of the highlighted finite elements ranges between 80% (blue elements) and 100% (red elements).

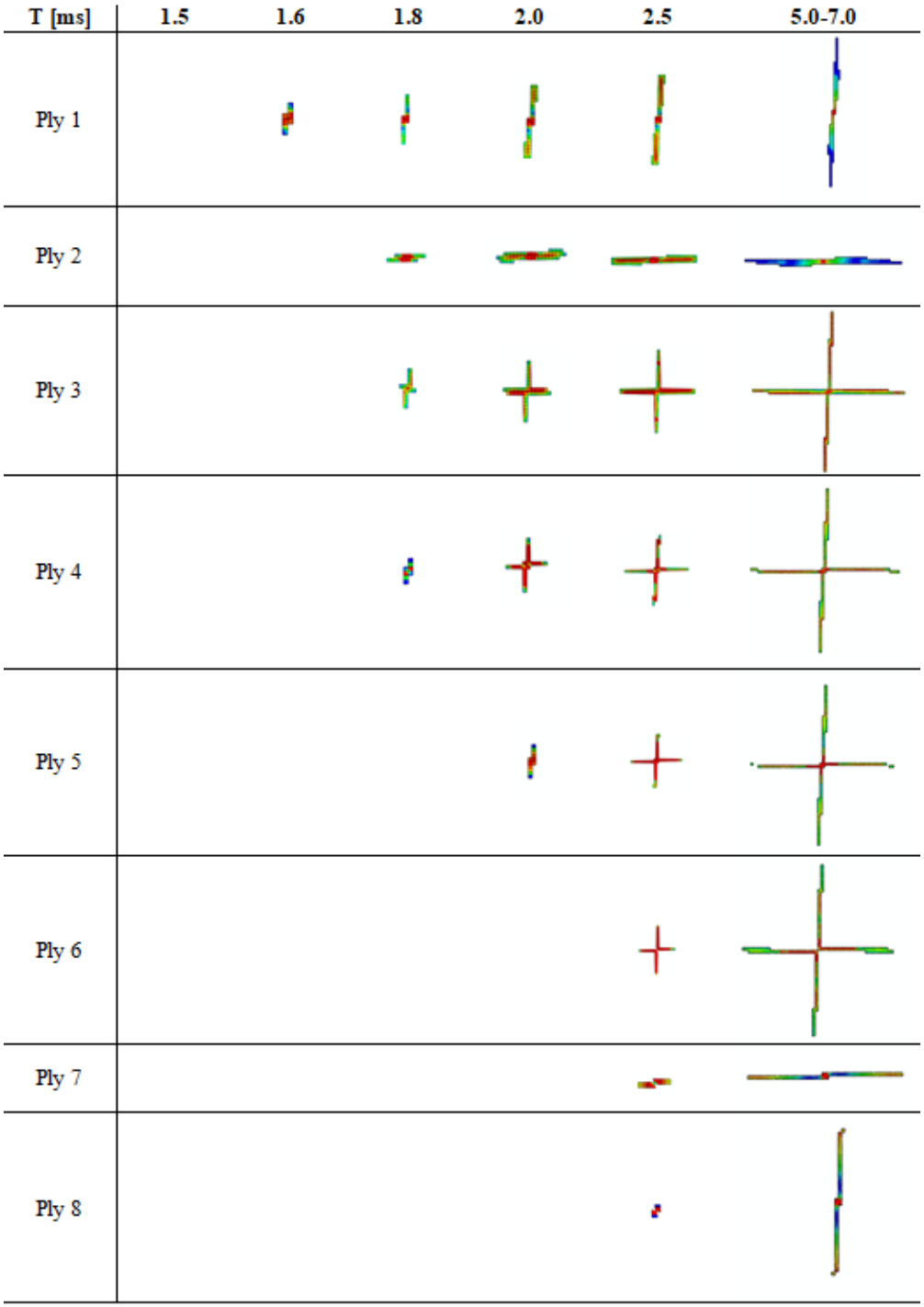

Table II. Fibre failures under tensile and compression loads.

T [ms]	1.5	1.6	1.8	2.0	2.5	5.0-7.0
Ply 1					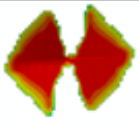	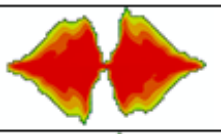
Ply 2				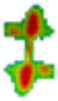		
Ply 3					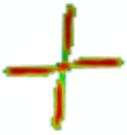	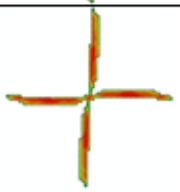
Ply 4						
Ply 5						
Ply 6						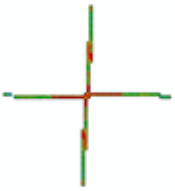
Ply 7						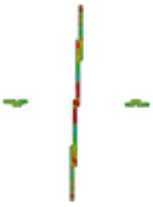
Ply 8						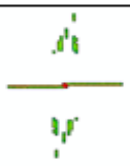

Table III. Matrix failures under tensile and compression loads.

According to Tables II and III, the damages configuration at the time increment 5 ms remains unchanged up to the end of the impact (7 ms).

In order to give an idea of the damages size shown in Tables II and III, the superimposition of all damages at the end of the impact simulation has been highlighted within the plate in Figure 4.a. Damages achieved in all time increments (Table II and III) have been reproduced in other six separate analogous plates; such six plates are characterized by the same geometries and the same mesh of the impacted one. So, damages have been manually reproduced by lowering the elastic material properties, lamina by lamina, in correspondence of the finite elements which, in the impacted plate, had been damaged.. The residual strength properties of each damaged lamina is different by each other, depending on the type of the damage mechanism (in matrix and/or the fibre) evolved. So the material properties are changed accordingly as a function of the damage type. If the damage evolution is in the matrix, the transverse Young modulus, E_{22}, and the shear modulus, G_{23}, are lowered by 80%; if the damage has initiated in the fibres, the longitudinal Young modulus, E_1, and the shear moduli, G_{12} and G_{13}, are reduced by 80%. If the integration points through the thickness are affected by both damage types, all aforementioned material properties are lowered by 80%.

The choice to lower the elastic material properties of 80% appears to be a reasonable strategy in the literature [12]. The area affected by a damage level greater than or equal to 80% can be considered fully damaged.

According to Figure 4.a, it can be noticed that damage is always initiated in the centre of the plate where it is surrounded by four piezoelectric (PZT) sensors located at the four corners 80 mm x 80 mm (Figure 4.b). After modelling the damage, Lamb wave propagation have been simulated on each of the six plates characterized by different damage configurations.

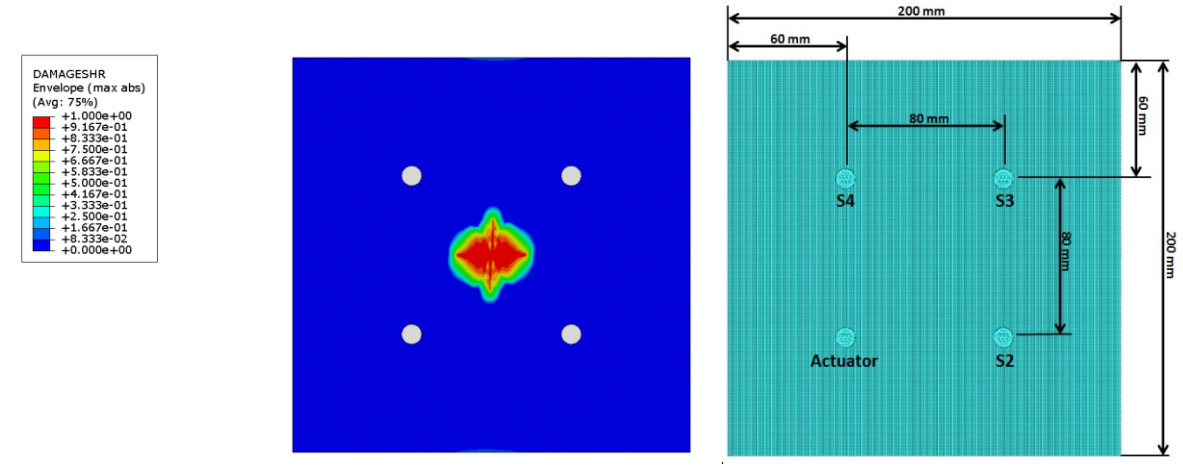

Figure 4. Damages configuration after the impact (a) and sensors location (b).

Figure 4.b, depicts the location of the actuator and the sensors on the plate. The sensors have been modelled by means of reduced integration solid elements (C3D8R, from the Abaqus elements' library; 3 dofs per node) and bonded to the plate by means of tie-constraints, which allow linking the degrees of freedom of the sensor elements to the plate. Each sensor is characterized by 8215 nodes and 6320 elements. The simulated transducers are characterized by the following material properties: E=70.5 GPa, v=0.33 and density ρ=7800 kg m^{-3}. The actuation signal is a five-cycle sine-burst signal. Furthermore, three central frequencies have been considered for the damage investigation: 150 kHz, 200 kHz and 250 kHz. Such signals have been numerically modelled by applying equivalent radial displacements to the actuator's upper edge [12, 30] (Figure 5), calculated from the analytical relation as a function of the Voltage [12]. The equivalent displacements can be achieved by means of Equation 1.

$$A = \frac{1}{2} V \left[1 - \cos\left(\frac{2\pi t f_c}{n}\right)\right] \sin(2\pi t f_c) \quad (1)$$

where, A is the amplitude, t is the wave propagating duration, f_c is the central frequency of the excitation signal, V is the maximum applied voltage and n is the number of cycles within the signal window (n=5).

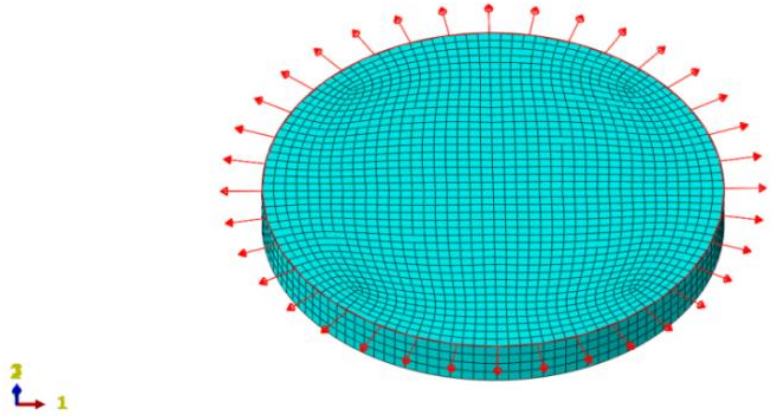

Figure 5. Actuation signal modelling.

Figures 6, 7 and 8 show the signals in Voltage and the related equivalent radial displacements for the central frequencies of 150 kHz, 200 kHz and 250 kHz, respectively.

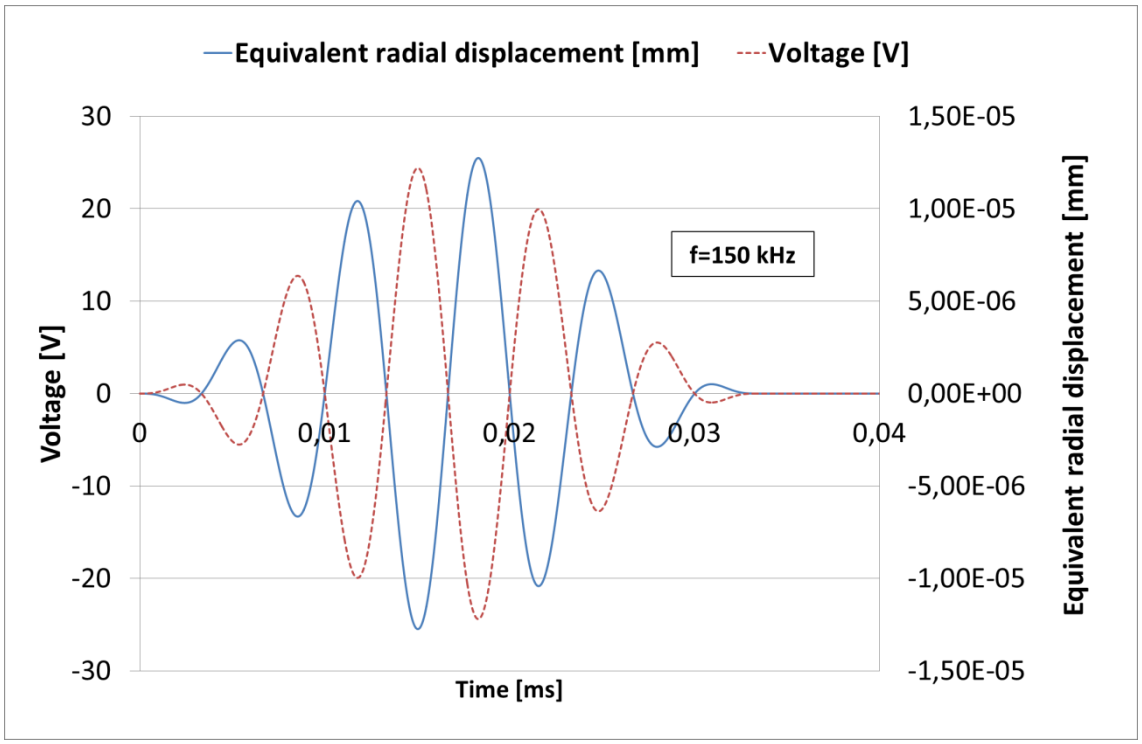

Figure 6. Actuator input voltage and equivalent radial displacement: *f*=150 kHz.

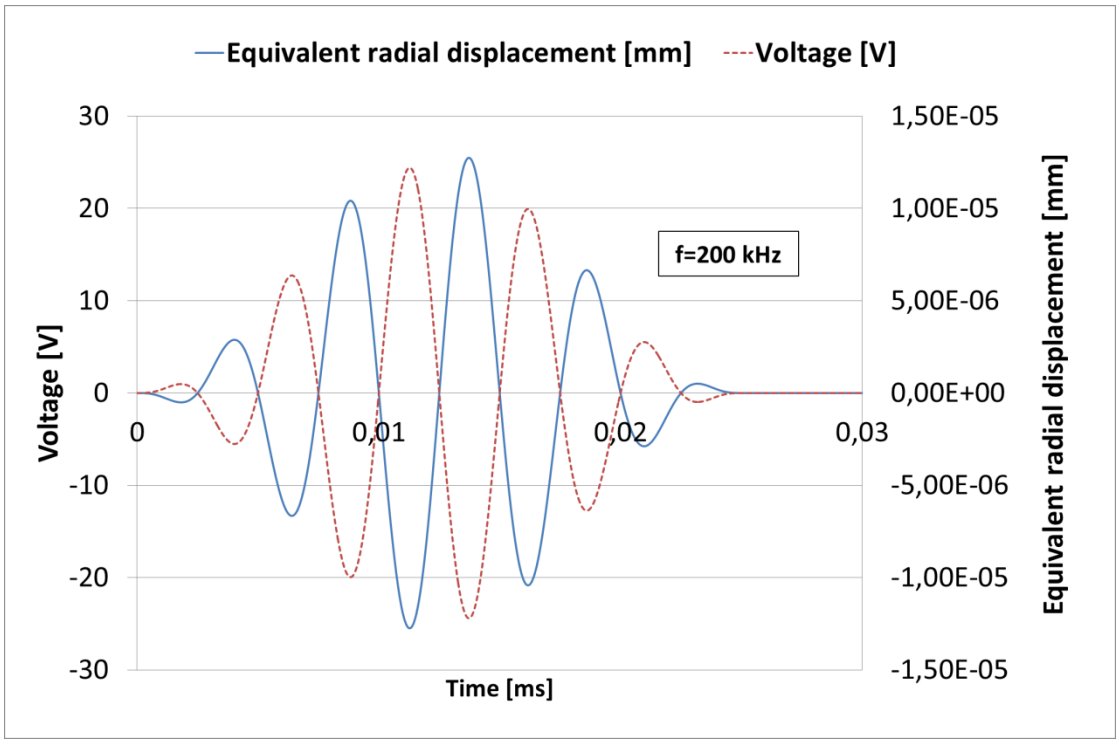

Figure 7. Actuator input voltage and equivalent radial displacement: *f*=200 kHz.

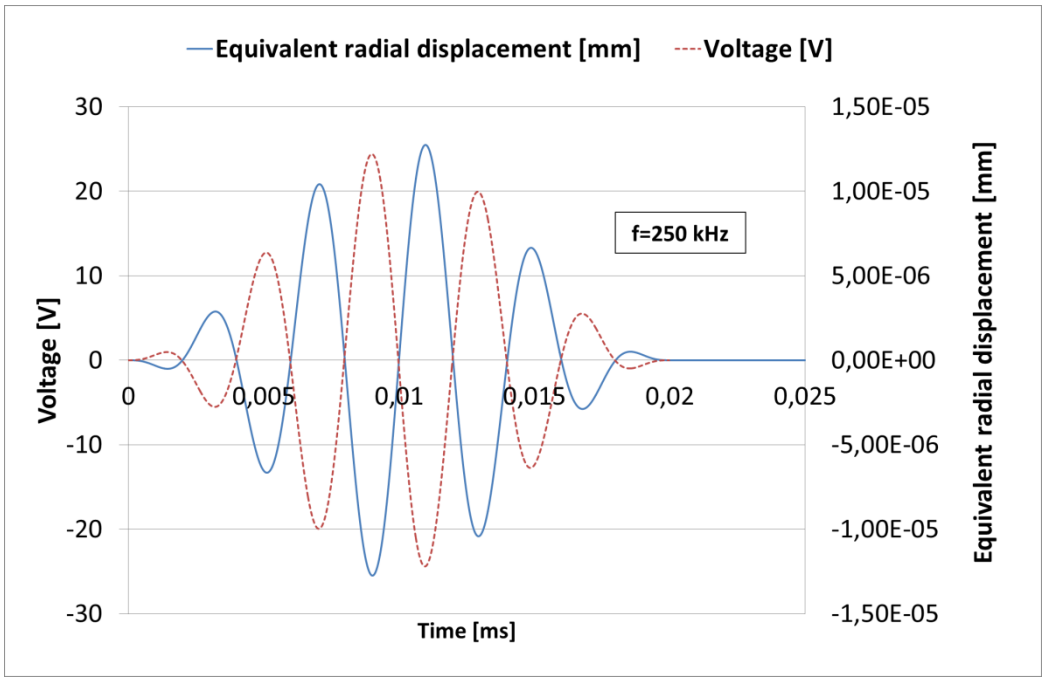

Figure 8. Actuator input voltage and equivalent radial displacement: *f*=250 kHz.

The wave propagation is a dynamic highly non-linear problem and the validity of the results depends on the correct mesh size and on the stable time increment, which is the minimum time that a dilatational wave takes to move across any element in the model and it can be calculated as the

ratio of the minimum distance of any two adjacent nodes to the maximum wave velocity (the explicit dynamics procedure solves every problem as a wave propagation problem; the solution can be obtained when the time increment is less than the stable time increment. Hence, it is important to estimate the stable time increment, in order to set a reasonable time increment). According to literature [18], in order to guarantee a good prediction of the wave propagation, the minimum value of the NPW is 15. In this work, 30 nodes per wavelength (NPW) have been considered for the analysis performed with the actuation signal characterized by the central frequency of 250 kHz. Moreover, since the mesh size for the three analysis types (150 kHz, 200 kHz and 250 kHz) has been kept unchanged, the analyses with central frequencies of 150 kHz and 200 kHz are characterized by more NPW (35 and 50, respectively); when the frequency decreases, the wavelength increases.

3.3 Wave-damage interaction: LVI damages representation based on Hashin criteria

As aforementioned, this second modelling strategy consists in the simulation of Lamb waves onto a plate characterized by an initial stress-strain state and the related failures carried out by a previous impact simulation. Before updating the stress-strain state due to the LVI and the respective failures as initial state of the plate in which Lamb wave propagation will be simulated, it is necessary to damp-out all vibrations produced by the impact. In fact, since the LVI is simulated by means of an explicit analysis, if no-damping factor is introduced in the material properties, the laminate will keep vibrating without reaching own equilibrium and the Lamb wave propagation will be performed on to a vibrating plate, where vibration amplitudes are bigger than the ones produced by the actuator.

By adding damping properties to the material, the computational costs of the LVI simulation increases. Therefore, in this section a different technique is proposed to damp-out such vibrations. The vibrations in the plate can also be damped out by introducing a load step after the LVI step,

characterized by the application of a viscous pressure on to the plate. The viscous pressure allows the plate to reach quasi-static equilibrium in a minimal number of increments and it can be defined through Equation 2:

$$p = -c_v v n \tag{2}$$

where p is the pressure applied to the body; c_v is the viscosity; v is the velocity vector of the point on the surface where the viscous pressure is being applied and n is the unit outward normal vector to the surface at the same point.

The choice of viscous pressure coefficient (c_v) is critical for using the technique effectively. Typically c_v is set equal to a small percentage (1% or 2%) of ρc_d (Equation 3):

$$\rho c_d = \rho \sqrt{\frac{E(1-v)}{\rho(1+v)(1-2v)}} \tag{3}$$

So when the velocity is equal to 0, the applied pressure is equal to 0. At the end of such load step, the energetic balance and the displacements of all plate nodes versus time appear on a quality level of the ones shown in Figure 9.

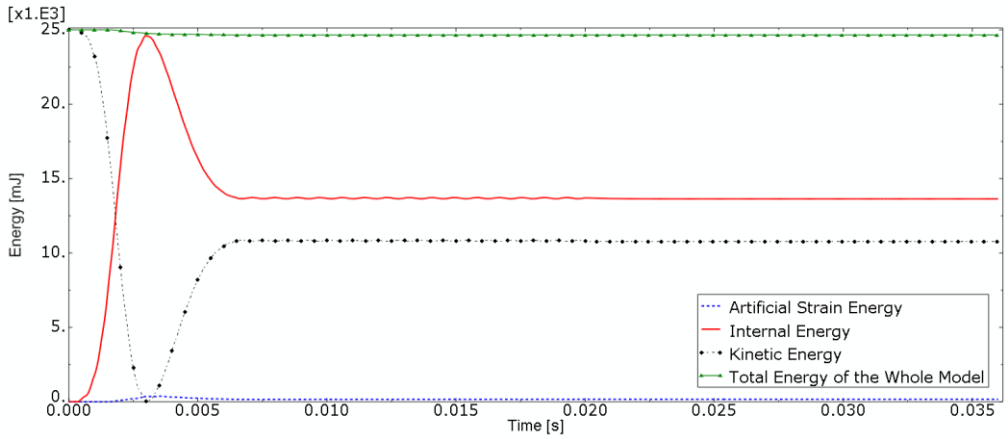

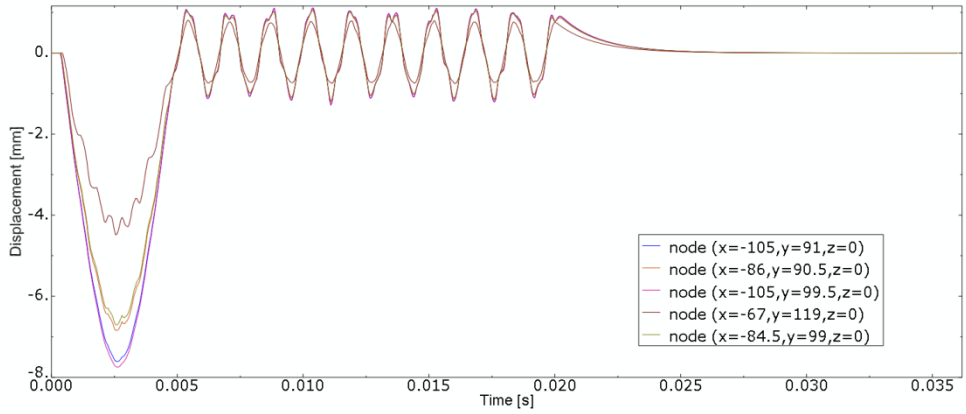

Figure 9. Energy balance [mJ] (a) and displacements versus time of five random nodes [s] (b).

According to Figure 9.b, for the sake of clarity, the displacements of only five random nodes of the plate have been plotted. The coordinates are referred to the reference system shown in Figure 2.a. After such step, the stress-strain state and the respective failures modelled by means of the LVI simulation can be imported as initial state of the plate, in which Lamb wave propagation will be simulated. It is important to highlight that also here, the simulation have been performed by means of an explicit formulation. An example of the Lamb wave propagation in the plate is shown as contour plots in Figure 10.

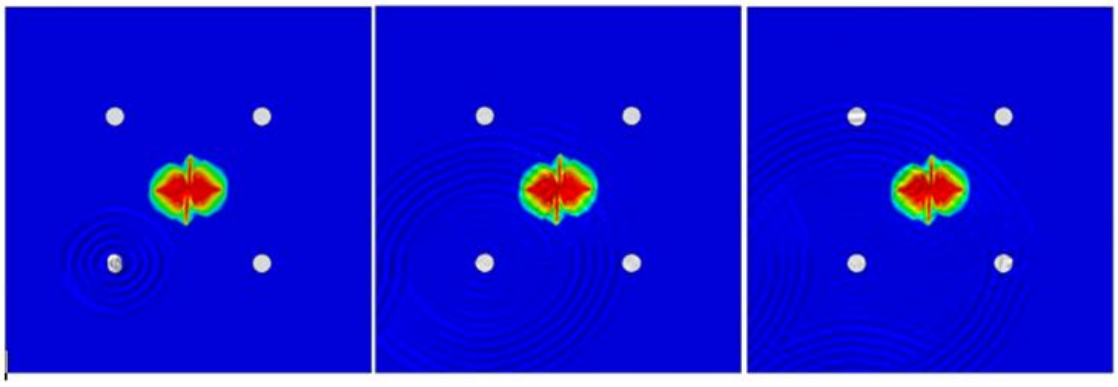

Figure 10. Lamb wave propagation in LVI damaged plate.

The damages shown in Figure 10 are the envelope along the thickness direction of all damages affecting the plate (fibre failures under both tensile and compressive load and matrix failure under both tensile and compressive load).

The interaction between the Lamb wave and such damages produces scattered waves, which allow detecting the presence of damages inside the plate.

In order to investigate the interaction between Lamb waves and different LVI damage configurations, five different impact energy levels have been considered: 5 J, 10 J, 15 J, 20 J and 25 J.

4 FE results.

It must be highlighted that all following post-processing analyses are related to an acquisition time of 0.1 ms after that the Lamb waves have been activated. This means that Lamb waves scattered by the plate boundary, according to Figure 11.d, do not reach sensor 3, but only sensors 2 and 4 (Figure 11.c).

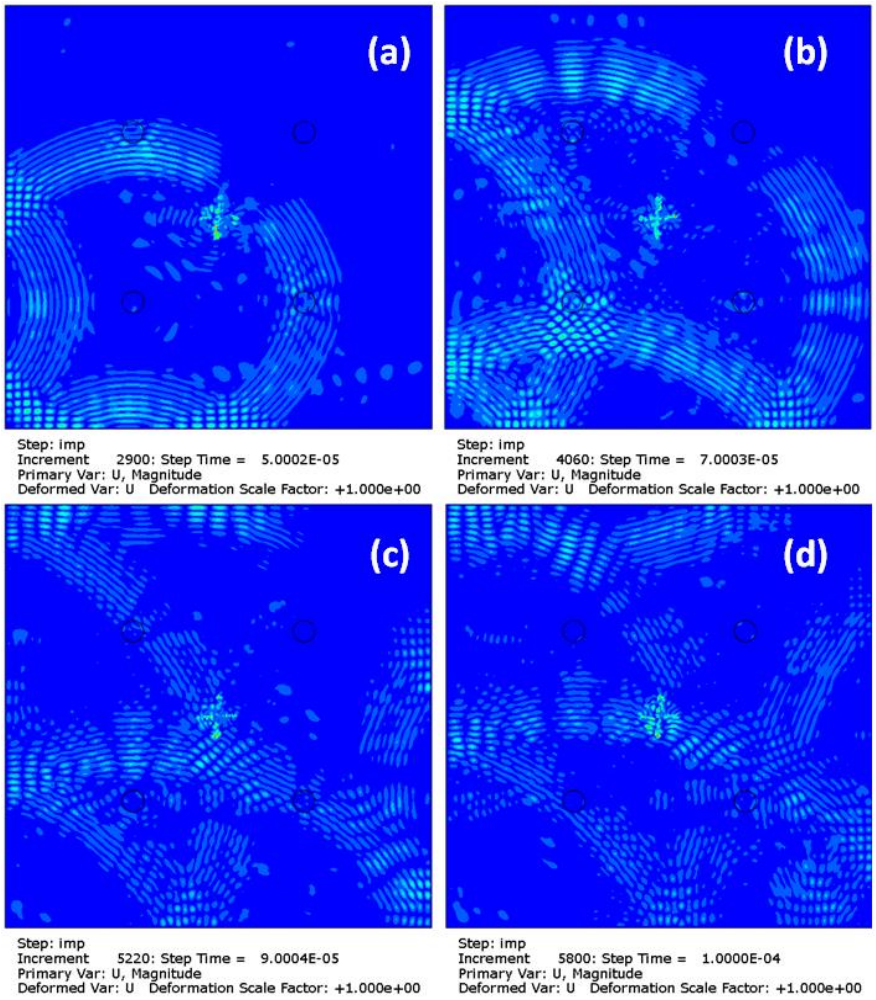

Figure 11. Frame sequence of the Lamb wave propagation in LVI damaged plate: 0.05 ms (a), 0.07 ms (b), 0.09 ms (c), 0.1 ms (d).

In more details, by considering such acquisition time, sensors will record both S_0 and A_0 modes (Section 2) and part of the boundary conditions scattered waves.

4.1 Modelling Strategy 1: analysis of results.

The RMSD damage index has been used to investigate the interaction between Lamb waves and damages at three different central frequencies of the actuation signal: 150 kHz, 200 kHz and 250 kHz, respectively shown in Figures 12, 13 and 14.

In each figure the RMSD damage indices obtained for each one of the six damages configurations and for each sensor have been shown. The damage index is a result of the comparison between each baseline sensor signal (reference configuration), and the sensor signals corresponding to each of the six damage configurations, respectively.

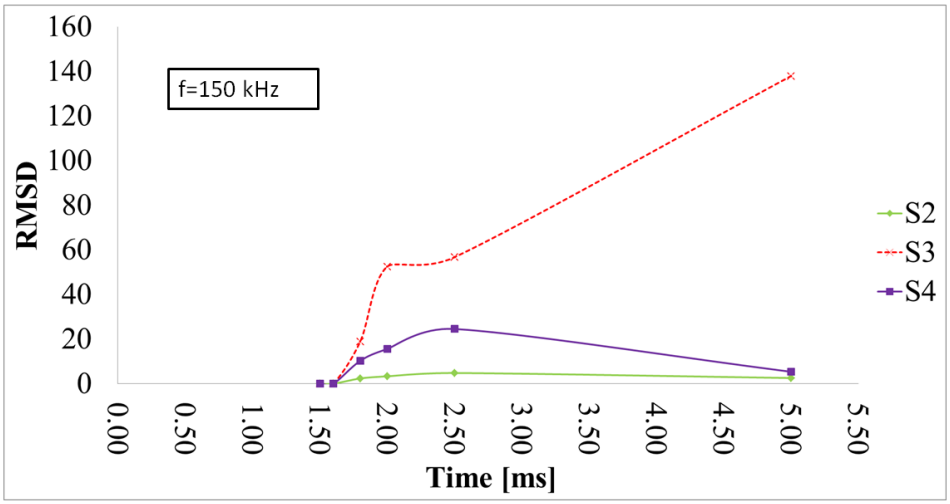

Figure 12. RMSD damage feature vs. time: actuation signal *f*=150 kHz.

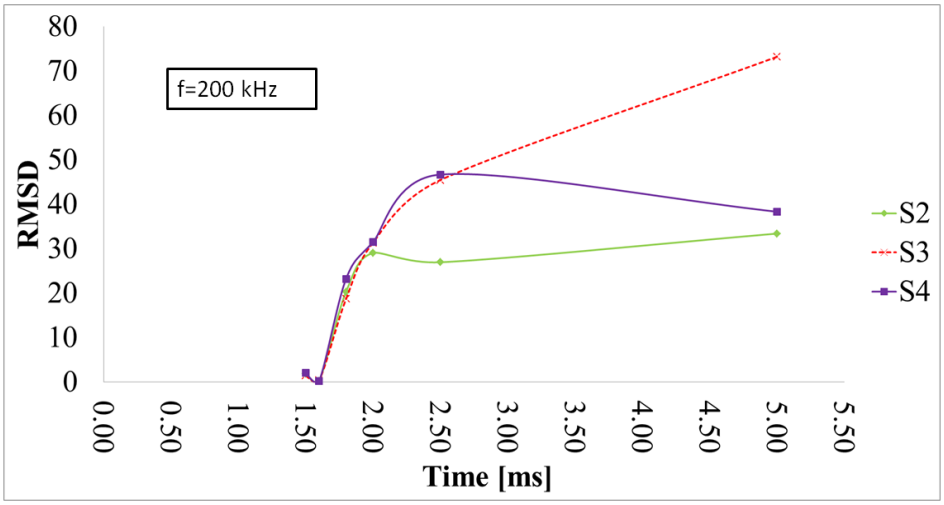

Figure 13. RMSD damage feature vs. time: actuation signal *f*=200 kHz.

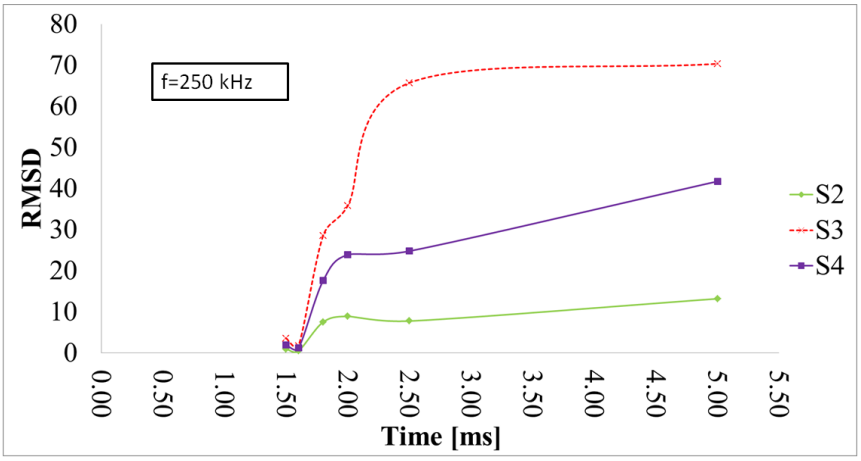

Figure 14. RMSD damage feature vs. time: actuation signal *f*=250 kHz.

According to Figures 12, 13 and 14, it can be noticed that the sensor 3 provides the highest values of the RMSD index, because, according to Figure 4, the propagation pattern is directly influenced by the presence of the damage. Moreover it can be observed from Figure 12 that the index values related to the other two sensors, which are indirectly affected by the damages, are much lower than the 3rd one. This is not true for the analyses in which the actuator has been excited with the central frequencies of 200 kHz and 250 kHz, (Figures 13 and 14).

According to Figure 13, it can be noticed that the RMSD index values of the three sensors, are, in terms of magnitude, comparable for all time instants of the impact history. It is interesting to notice that, with a central frequency of 200 kHz, the three sensors provide the same RMSD index values for the first four time instants (1.5 ms, 1.6 ms, 1.8 ms and 2.0 ms). Contrary to the other performed analyses (150 kHz and 250 kHz), the RMSD curves are initially characterized by the same slope. Moreover, by comparing the three graphs (Figures 12, 13 and 14) from a qualitative point of view, it appears that sensor 2, which is placed along the first lamina fibres direction, generally provides the lowest values of the RMSD index. Concerning Figure 14, it can be noticed that the RMSD curves are generally characterized by the same trend which helps understand the damage mechanisms during a LVI event. From this comparison it can be concluded that, since in real application damage can evolve in any part of a component, the best solution to activate Lamb waves

SHM system consists in finding, rather than the optimal sensors locations, the central frequency of the actuation signal providing comparable values of the damage indexes for all sensors surrounding the damage. In this way, it may be possible to achieve important information by all sensors independent of the fibres orientation.

Other considerations can be made from a qualitative point of view by plotting the RMSD values as a function of the envelope damage size assessed at the different instants of the impact history. According to Figure 15, it appears that the 150 kHz actuation signal is too weaker for damage detection purposes and this result in values of the RMSD index too much lower for the sensor 2. Accordingly, if the damage detection task were assigned only to sensor 2, the result of the damage detection phase would be negative.

From Figure 16, it can be noticed that the 200 kHz analysis provides comparable values of the RMSD index for the three sensors. Moreover, the curves are firstly characterized by the same trend and slope, up to almost 100 mm^2, and then by different trends. According to Figure 17, achieved by considering a central frequency of the actuation signal of 250 kHz (which allows to increase the damage detectability, due to the lower wavelengths), it can be noticed that the overall trend of the RMSD values obtained for the three sensors is almost similar and essentially characterized by three macro-phases. The first one, where the RMSD increases sharply as the damage appears and, more in detail, this phase involves also the first instants of the damage evolution (from 0 mm^2 to 50 mm^2); the second one, characterized by a lower slope of the curves up to they get almost constant as the damage size increases (from 120 mm^2 to 270 mm^2); the third one, where the RMSD curves start to increase again, but more smoothly than the first phase. The damage index does not increase linearly with the damage size, but it reflects indirectly the failure mechanisms beyond the damage onset and evolution. By comparing Figures 3 and 17, the three different slopes can be linked to the three phases of the impact history: Phase I: the impactor contacts the plate; Phase II: the impactor reaches its maximum displacement, the latter, and Phase III: is related to the elastic response of the plate.

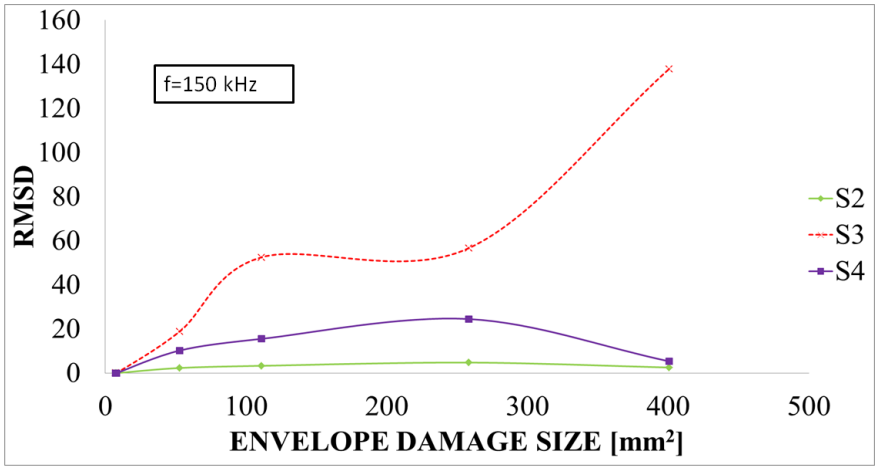

Figure 15. RMSD damage feature vs. envelope damage size: actuation signal *f*=150 kHz.

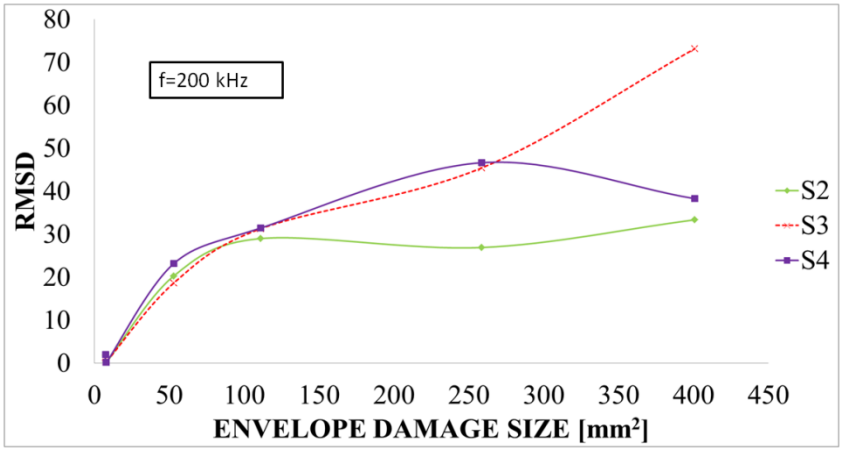

Figure 16. RMSD damage feature vs. envelope damage size: actuation signal *f*=200 kHz.

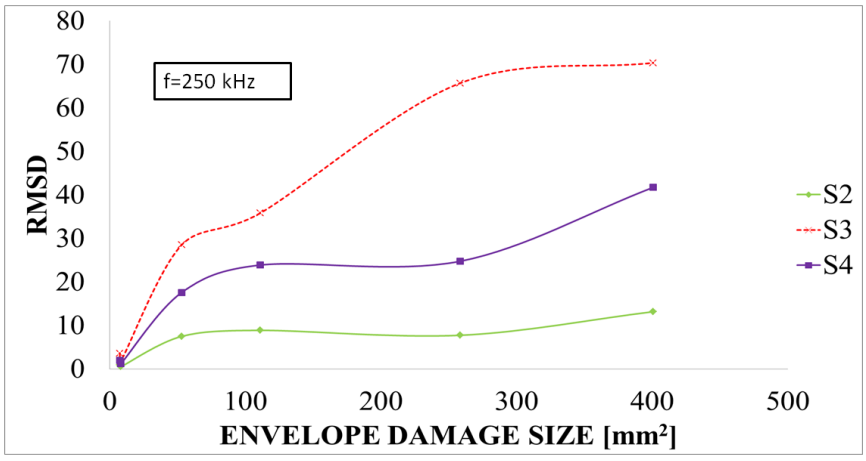

Figure 17. RMSD damage feature vs. envelope damage size: actuation signal *f*=250 kHz.

4.2 Modelling Strategy 2: analysis of results.

Regarding the second modelling strategy, an investigation similar to the previous one has been performed with the main attempt to assess the Lamb wave propagation at different impact energy levels.

The RMSD index values, for the three sensors, have been plotted as a function of the impact energy level. Figures 18, 19 and 20 show the RMSD index values achieved by the three sensors for the 150 kHz, 200 kHz and 250 kHz actuation signals, respectively. Moreover, in the same figures, for each impact energy level it has been pointed out the contour plot of a section of the laminate (45 mm x 45 mm) showing the failures produced by the impact. Moreover, for each impact energy level, the left contour plot shows the impacted surface of the laminate, whilst the right one shows the bottom surface. According to each contour plot, the superimposition of all Hashin failures (fibre and matrix failures under tensile and compressive loads) has been shown. The red finite elements are those completely damaged; the orange/yellow finite elements are those characterized by a stiffness lowering of 65% ÷ 90%; the green finite elements are those characterized by a stiffness lowering of 30%÷65%; the blue finite elements are those completely undamaged.

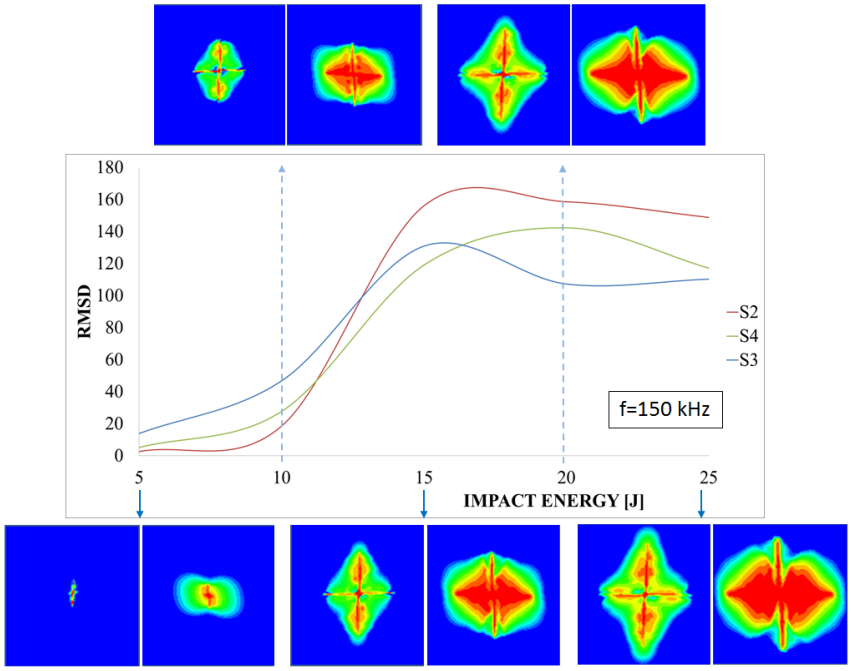

Figure 18. RMSD damage feature vs. impact energy levels: actuation signal *f*=150 kHz.

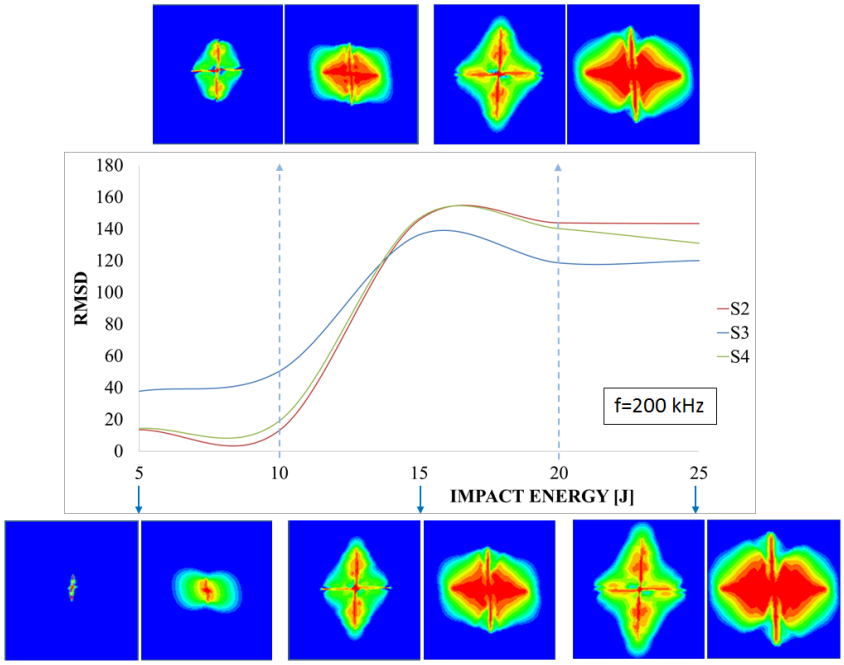

Figure 19. RMSD damage feature vs. impact energy levels: actuation signal *f*=200 kHz.

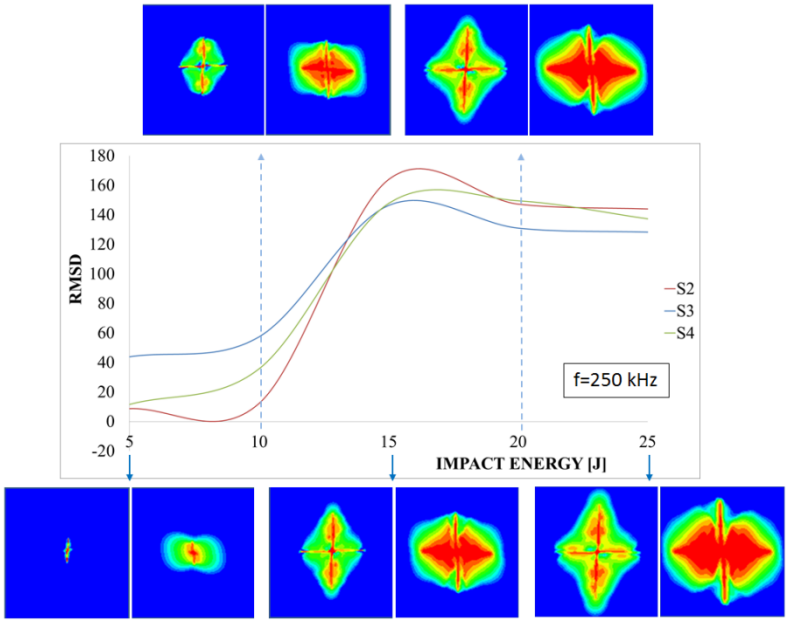

Figure 20. RMSD damage feature vs. impact energy levels: actuation signal *f*=250 kHz.

According to the three Figures 18, 19 and 20, the overall trend of the RMSD index values as a function of the impact energy level is expressible by means of a sort of "S" curve. The Lamb waves appear to be more sensitive for impact energy levels higher than 10 J. After that, the RMSD index increases dramatically to reach a peak in correspondence to the 15 J impact energy level. The

following values of RMSD index are characterized by a light decrease, after which they remain almost constant. The increase of the RMSD index between 10 J and 15 J impact energy levels is due to the different damage configurations. The difference in terms of damage size between the 10 J and 15 J impact energy levels is larger than the other differences between two consecutive values. Moreover, as shown in Figures 19, it can be noticed that, similar to results from modelling strategy 1, the RMSD curves achieved by sensors 2 and 4 are quite overlapped; under such approach, however, the overlapping exists for all damages configurations. This may be attributed to the better damage modelling technique. Under the first modelling strategy, the damage modelling may be affected by significant approximations. As a result, it can be concluded that the actuation signal with central frequency of 200 kHz, for the specific test case, is the best among the investigated ones for damage detection purpose. Under such frequency there is not the effect of the fibres orientation on the damage detection.

4.3 Comparison of the techniques.

In this section a comparison between the two investigated techniques is proposed. As aforementioned in Section 1, the softening representation introduces several approximations in the damage modelling; the lowering of the elastic material properties leads to a bad damage modelling which does not allow reproducing properly what happens in the reality. However, nowadays, such technique appears to be the most adopted one in the literature. The modelling of the interaction between Lamb waves and damages is so complex that such approximations are usually well accepted.

In order to estimate the approximation level, in this paper the results achieved by the first technique are compared with the second strategy ones (LVI damages representation). Such technique allows a better damage modelling and, consequently, overcoming the damage modelling approximations introduced by the softening strategy (usually used in literature). In fact, as described in Section 4.2, in order to better model the interactions between Lamb waves and LVI damages, such damages are

modelled in a previous impact simulation, by introducing in the FE model the Hashin criteria which are established and more accurate.

The results comparison is carried out by comparing the RMSD index values achieved by both strategies under the 25 J energy level damage configuration for the three considered central frequencies (150 kHz, 200 kHz and 250 kHz). In particular, Figures 21, 22 and 23 compare the RMSD index values predicted by sensor 2, 3 and 4, respectively.

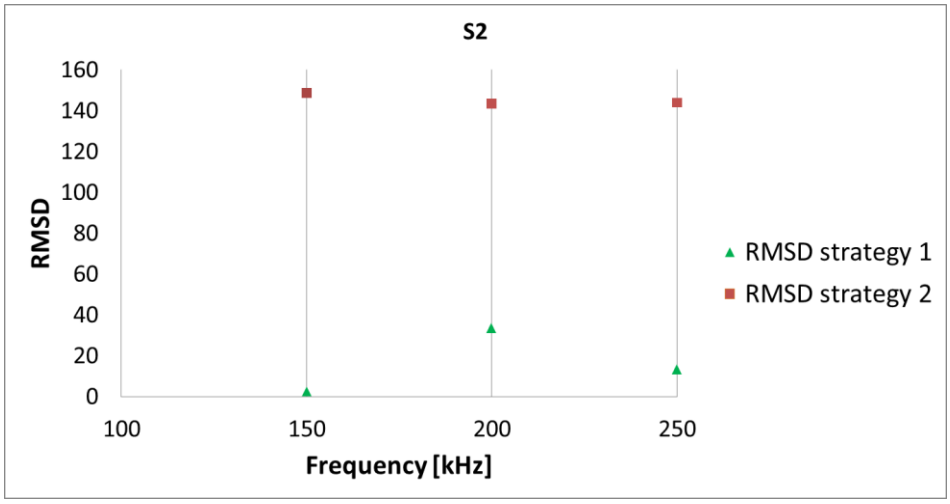

Figure 21. Comparison between strategies: RMSD recorded at sensor 2 under the 25 J damage configuration.

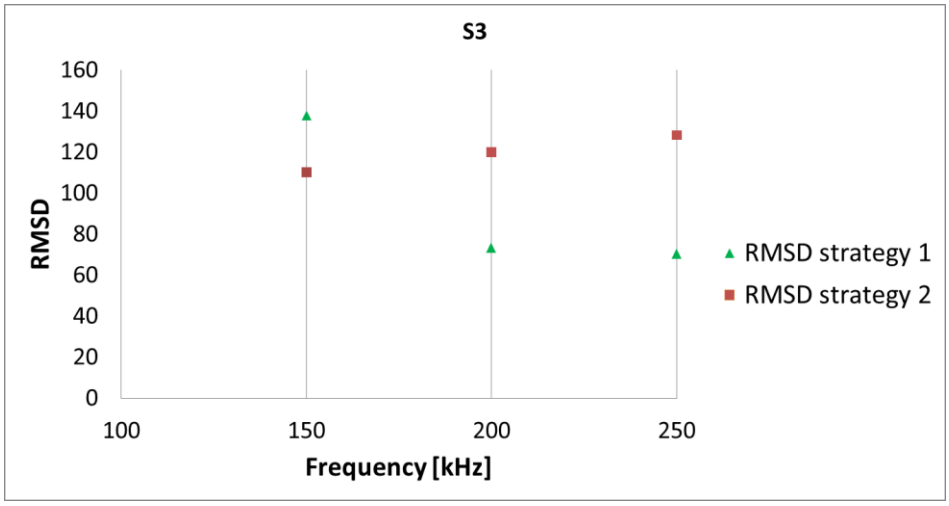

Figure 22. Comparison between strategies: RMSD recorded at sensor 3 under the 25 J damage configuration.

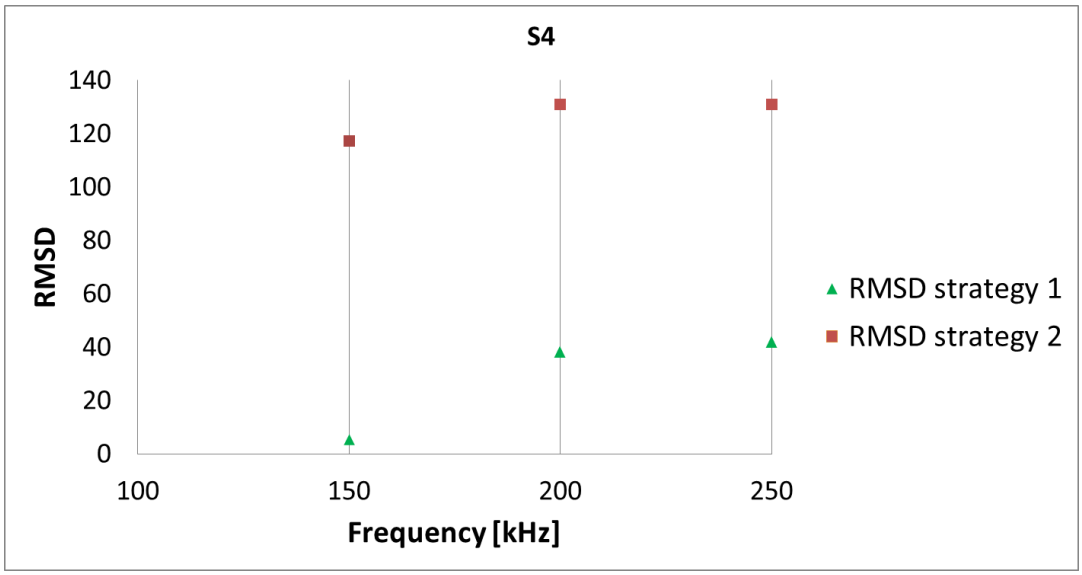

Figure 23. Comparison between strategies: RMSD recorded at sensor 4 under the 25 J damage configuration.

According to Figures 21, 22 and 23, it can be noticed that the RMSD index values predicted by both strategies are completely in disagreement. It can be noticed that the RMSD index values predicted by strategy 2 are always higher than strategy 1 ones, except for the analysis with central frequency of 150 kHz. Sensor 3, in fact, predicts a RMSD index value which is lower.

The reasons of the disagreement between the two techniques can be attributed to the approximations introduced by strategy 1. Moreover, strategy 2, conversely to strategy 1, allows introducing in the plate where the Lamb waves are activated, rather than the LVI damages, also the stress-strain state related to the presence of such damages. In addition, strategy 1 does not give the possibility to consider the different shape characterizing the plate after the impact phenomenon respect to the undamaged one (indentation, deformations,…). According to Figure 22, it can be also observed that the differences between the RMSD index values predicted by sensor 3 in both strategies decrease. This is due to the fact that the damages modelled according to both strategies interrupt in a similar way the pattern between the actuator and sensor 3.

5 Conclusions.

In this work Lamb wave interaction with several LVI damages configurations has been extensively investigated numerically. Two FE techniques for the LVI damages modelling have been presented allowing understanding the effects of Lamb wave propagation during the onset and the evolution of LVI damages and the effects of Lamb waves under several impact energy levels, respectively. Moreover, the interaction between Lamb waves and damages has been investigated under three central frequencies of the actuation signal: 150 kHz, 200 kHz and 250 kHz. As a result of such investigation, the importance of the actuation frequency for damage detection purposes has been shown. For the presented test case, it appeared that only the 200 kHz central frequency allowed achieving the same value of damage index in correspondence to the sensors surrounding the damage, even if located with different orientations with respect to the first lamina's fibres orientation.

Finally the comparison between the results achieved by the two investigated techniques has been presented. The results appear completely in disagreement by showing the need to use a more accurate technique for the damage modelling. Relatively to the modelling of the interaction between Lamb waves and LVI damages, a new procedure has been presented within such paper to overcome the approximations introduced by the softening representation, which is, currently, the most used in literature. However, further experimental investigations are needed to assess which technique gives more accurate information on the interaction between Lamb waves and LVI damages.

References

[1] Sepe R, Citarella R, De Luca A, Aremntani A. Numerical and Experimental Investigation on the Structural Behaviour of a Horizontal Stabilizer under Critical Aerodynamic Loading Conditions.

[2] Caputo F, Lamanna G, De Luca A, Lopresto V. Numerical simulation of LVI test onto composite. AIP Conference Proceedings 2014; 1599: 334-337.

[3] Riccio A, Sellitto A, Saputo A, Russo A, Zarrelli M, Lopresto V. Modelling the damage evolution in notched omega stiffened composite panels under compression. Compos Part B - Eng 2017;126: 60-71.

[4] Riccio A, Russo A, Sellitto A, Raimondo A. Development and application of a numerical procedure for the simulation of the “Fibre Bridging” phenomenon. Compos Struct 2017; 168: 104-119.

[5] Riccio A, Saputo S, Sellitto A, Raimondo A, Ricchiuto R. Numerical investigation of a stiffened panel subjected to low velocity impacts. Key Eng Mat 2016; 665: 277-280

[6] Borrelli R, Riccio A, Sellitto A, Caputo F, Ludwig T. On the use of global-local kinematic coupling approaches for delamination growth simulation in stiffened composite panels. Science and Technology 2015; 115: 43-51

[7] Liu D. Impact-induced delamination - A view of bending stiffness mismatching. J Compos Mater 1998; 22: 674-92.

[8] Sepe R, De Luca A, Lamanna G, Caputo F. Numerical and experimental investigation of residual strength of a LVI damaged CFRP omega stiffened panel with a cut-out. Compos Part B – Eng 2016; 102: 38-56.

[9]. Abrate S. Impact on composite structures. Cambridge University Press. Cambridge (1998).

[10] Certification Specifications for Large Aeroplanes CS-25. European Aviation Safety Agency, Amendment 5, 5 September 2008.

[11] Mircea Calomfirescu, Holger Hickethier. Damage tolerance of composite structures in aircraft industry. Internal Technical Report EADS – Defence and Security (2010).

[12] Su Z, Ye L. Identification of Damage Using Lamb Waves. Applied and Computational Mechanics 2009; 48.

[13]Lee B C, Staszewski W J. Modelling of Lamb waves for damage detection in metallic structures: part I – wave propagation. Smart Mater Struct 2003; 12: 804-814.

[14] Yelve N P, Mitra M, Mujumdar P M, Detection of delamination in composite laminates using Lamb wave based nonlinear method, Compos Struct 2017; 159: 257–266.

[15] Mustapha S, Ye L. Propagation behaviour of guided waves in tapered sandwich structures and debonding identification using time reversal. Wave Motion 2015; 57: 154–170.

[16] Hennings B, Lammering R. Material modeling for the simulation of quasi-continuous mode conversion during Lamb wave propagation in CFRP-layers. Compos Struct 2016; 151 142–148.

[17] Ng C T, Veidt M,. Rose L R F, Wang C H. Analytical and finite element prediction of Lamb wave scattering at delaminations in quasi-isotropic composite laminates. J Sound Vib 2012; 331: 4870–4883.

[18] Sharif-Khodaei Z Aliabadi M H. Assessment of delay-and-sum algorithms for damage detection in aluminium and composite plates. Smart Mater Struct 2014; 23 (2014) 075007 (20pp).

[19] Wang Y, Guan R, Lu Y. Nonlinear Lamb waves for fatigue damage identification in FRP reinforced steel plates. Ultrasonics 2017; 80: 87–95

[20]Ben B, Ben B A, Kothapalli A V, Yang S H. Damage identification in composite materials using ultrasonic based Lamb wave method Measurement 2012; 46: 904–12

[21] Diamanti K, Soutis C, Hodgkinson J M. Lamb waves for the non-destructive inspection of monolithic and sandwich composite beams. Compos Part A- Appl S 2005; 36 189–95

[22] Fromme P, Wilcox P D, Lowe M J S, Cawley P. On the development and testing of a guided ultrasonic wave array for structural integrity monitoring IEEE Trans. Ultrason Ferroelectr Freq Control 2006; 53: 777–85

[23] Kudela P, Ostachowicz W, Zak A. Damage detection in composite plates with embedded PZT transducers. Mech Syst Signal Process 2008; 22: 1327–35

[24] Kudela P, Arkadiusz, Ak, Ostachowicz Aw. Modelling of wave propagation in composite plates using the time domain spectral element method. J Sound Vib 2007; 302: 728–45

[25] Michaels J. Detection, localization and characterization of damage in plates with an in situ array of spatially distributed ultrasonic sensors. Smart Mater Struct 2008; 17: 035035

[26] Michaels J E, Michaels T E. Guided wave signal processing and image fusion for in situ damage localization in plates. Wave Motion 2007; 44: 482–92

[27] Ostachowicz W, Kudela P, Malinowki P, Wandoswsi T. Damage localisation in plate-like structures based on PZT sensors. Mech Syst Signal Process 2009; 23: 1805–29.

[28] Sharif-Khodaei Z, Ghajari M, Aliabadi M H. Determination of impact location on composite stiffened panels. Smart Mater Struct 2012; 21: 105026 (14pp).

[29] Hashin Z. Failure criteria for unidirectional composites. Journal Applied Mechanism 1980;47:329-334.

[30] De Luca A, Sharif-Khodaei Z, Aliabadi M H, Caputo F. Lamb Wave Propagation in Impacted CFRP. Procedia Engineering 2016; 167: 109-115.